Delocalization of wave packets in disordered nonlinear chains

Ch. Skokos,[1] D. O. Krimer,[1] S. Komineas,[2] and S. Flach[1]
[1]*Max Planck Institute for the Physics of Complex Systems, Nöthnitzer Straße 38, D-01187 Dresden, Germany*
[2]*Department of Applied Mathematics, University of Crete, Heraklion, Crete GR-71409, Greece*
(Received 27 January 2009; published 12 May 2009)

We consider the spatiotemporal evolution of a wave packet in disordered nonlinear Schrödinger and anharmonic oscillator chains. In the absence of nonlinearity all eigenstates are spatially localized with an upper bound on the localization length (Anderson localization). Nonlinear terms in the equations of motion destroy the Anderson localization due to nonintegrability and deterministic chaos. At least a finite part of an initially localized wave packet will subdiffusively spread without limits. We analyze the details of this spreading process. We compare the evolution of single-site, single-mode, and general finite-size excitations and study the statistics of detrapping times. We investigate the properties of mode-mode resonances, which are responsible for the incoherent delocalization process.

DOI: 10.1103/PhysRevE.79.056211 PACS number(s): 05.45.−a, 05.60.Cd, 63.20.Pw

I. INTRODUCTION

The normal modes (NMs) of a $d=1$-dimensional linear system with uncorrelated random potential are spatially localized (Anderson localization). Therefore any wave packet, which is initially localized, remains localized for all time [1]. Note that NMs correspond to single-particle eigenstates of related quantum systems.

When nonlinearities are added, NMs interact with each other [2]. Recently, experiments were performed on light propagation in spatially random nonlinear optical media [3,4] and on Bose-Einstein condensate expansions in random optical potentials [5], which serve as realizations of such cases.

Numerical studies of wave packet propagation in several models showed that the second moment of the norm/energy distribution grows subdiffusively in time as t^{α} [6–9], with $\alpha \approx 1/3$ for $d=1$. Reports on partial localization were published as well [10].

In a recent paper the mechanisms of spreading and localization were studied for $d=1$, with initial excitations being localized on a single site [11]. A theoretical explanation of the exponent $\alpha=1/3$ was obtained, consistently assuming that the internal dynamics of a wave packet is chaotic, leading to a partial dephasing of the NMs. The argumentation was based on the possibility of a pair of wave-packet modes being able to resonantly interact with each other. Among other results, the case of weak nonlinearity showed that wave packets localize according to the linear dynamics on long but finite time scales, with subsequent detrapping. In the present work, we extend this study to single-mode excitations and more general excitations of width L. We study the details of the detrapping process and measure the statistical properties of detrapping times. We study the particularities of resonant interaction between modes mediated by the nonlinearity. We give details on the used integration schemes and perform extensive tests which demonstrate that the observed effects are not affected by round-off errors. We argue that the spreading is inherently induced by the nonintegrability of the system.

II. MODELS

We study two models of one-dimensional lattices.

A. Nonlinear Schrödinger lattice

The Hamiltonian of the disordered discrete nonlinear Schrödinger equation (DNLS)

$$\mathcal{H}_D = \sum_l \epsilon_l |\psi_l|^2 + \frac{\beta}{2}|\psi_l|^4 - (\psi_{l+1}\psi_l^* + \psi_{l+1}^*\psi_l), \tag{1}$$

with complex variables ψ_l, lattice site indices l and nonlinearity strength $\beta \geq 0$. The random on-site energies ϵ_l are chosen uniformly from the interval $[-\frac{W}{2}, \frac{W}{2}]$, with W denoting the disorder strength. The equations of motion are generated by $\dot{\psi}_l = \partial \mathcal{H}_D / \partial(i\psi_l^*)$:

$$i\dot{\psi}_l = \epsilon_l \psi_l + \beta|\psi_l|^2\psi_l - \psi_{l+1} - \psi_{l-1}. \tag{2}$$

Equation (2) conserve the energy [Eq. (1)] and the norm $S = \Sigma_l |\psi_l|^2$. We note that varying the norm of an initial wave packet is strictly equivalent to varying β, therefore we choose $S=1$. Equations (1) and (2) are derived, e.g., when describing two-body interactions in ultracold atomic gases on an optical lattice within a mean-field approximation [12] but also when describing the propagation of light through networks of coupled optical waveguides in Kerr media [13].

For $\beta=0$ Eq. (1) with $\psi_l = A_l \exp(-i\lambda t)$ is reduced to the linear eigenvalue problem

$$\lambda A_l = \epsilon_l A_l - A_{l-1} - A_{l+1}. \tag{3}$$

The normalized eigenvectors $A_{\nu,l}$ ($\Sigma_l A_{\nu,l}^2 = 1$) are the NMs, and the eigenvalues λ_ν are the frequencies of the NMs. The width of the eigenfrequency spectrum λ_ν of Eq. (3) is $\Delta_D = W+4$ with $\lambda_\nu \in [-2-\frac{W}{2}, 2+\frac{W}{2}]$.

The asymptotic spatial decay of an eigenvector is given by $A_{\nu,l} \sim e^{-l/\xi(\lambda_\nu)}$, where $\xi(\lambda_\nu) \leq \xi(0) \approx 100/W^2$ is the localization length [14]. The NM participation number $p_\nu = 1/\Sigma_l A_{\nu,l}^4$ characterizes the spatial extend (localization volume) of the NM. It is distributed around the mean value $p_\nu \approx 3.6\xi(\lambda_\nu)$ with variance $\approx 1.3\xi(\lambda_\nu)$ [15]. The average spac-

 ©2009 The American Physical Society

ing of eigenvalues of NMs within the range of a localization volume is therefore $\overline{\Delta\lambda}_D \approx \Delta_D/p_\nu \approx \Delta_D W^2/360$. The two scales $\overline{\Delta\lambda}_D \leq \Delta_D$ determine the packet evolution details in the presence of nonlinearity.

The equations of motion of Eq. (1) in normal-mode space read as

$$i\dot{\phi}_\nu = \lambda_\nu \phi_\nu + \beta \sum_{\nu_1,\nu_2,\nu_3} I_{\nu,\nu_1,\nu_2,\nu_3} \phi^*_{\nu_1} \phi_{\nu_2} \phi_{\nu_3}, \tag{4}$$

with the overlap integral

$$I_{\nu,\nu_1,\nu_2,\nu_3} = \sum_l A_{\nu,l} A_{\nu_1,l} A_{\nu_2,l} A_{\nu_3,l}. \tag{5}$$

The variables ϕ_ν determine the complex time-dependent amplitudes of the NMs.

The frequency shift of a single-site oscillator induced by the nonlinearity is $\delta_l = \beta |\psi_l|^2$. If instead a single mode is excited, its frequency shift is given by $\delta_\nu = \beta |\phi_\nu|^2 / p_\nu$.

B. Anharmonic oscillator lattice

The Hamiltonian of the quartic Klein-Gordon (KG) lattice

$$\mathcal{H}_K = \sum_l \frac{p_l^2}{2} + \frac{\tilde{\epsilon}_l}{2} u_l^2 + \frac{1}{4} u_l^4 + \frac{1}{2W} (u_{l+1} - u_l)^2, \tag{6}$$

where u_l and p_l are, respectively, the generalized coordinates and momenta, and $\tilde{\epsilon}_l$ are chosen uniformly from the interval $[\frac{1}{2}, \frac{3}{2}]$. The equations of motion are $\ddot{u}_l = -\partial \mathcal{H}_K / \partial u_l$ and yield

$$\ddot{u}_l = -\tilde{\epsilon}_l u_l - u_l^3 + \frac{1}{W}(u_{l+1} + u_{l-1} - 2u_l). \tag{7}$$

Equation (7) conserve the energy [Eq. (6)]. They serve, e.g., as simple models for the dissipationless dynamics of anharmonic optical lattice vibrations in molecular crystals [16]. The energy of an initial state $E \geq 0$ serves as a control parameter of nonlinearity similar to β for the DNLS case.

The coefficient $1/(2W)$ in Eq. (6) was chosen so that the linear parts of Hamiltonians (1) and (6) would correspond to the same eigenvalue problem. In practice, for $E \to 0$ (or by neglecting the nonlinear term $u_l^4/4$) model (6) with $u_l = A_l \exp(i\omega t)$ is reduced to the linear eigenvalue problem [Eq. (3)] with $\lambda = W\omega^2 - W - 2$ and $\epsilon_l = W(\tilde{\epsilon}_l - 1)$. The width of the squared frequency ω_ν^2 spectrum is $\Delta_K = 1 + \frac{4}{W}$ with $\omega_\nu^2 \in [\frac{1}{2}, \frac{3}{2} + \frac{4}{W}]$. Note that $\Delta_D = W\Delta_K$. As in the case of DNLS, W determines the disorder strength.

The spatial properties of the NMs are identical with those of Eq. (3). In addition to the scale Δ_K, the average spacing of squared eigenfrequencies of NMs within the range of a localization volume is $\overline{\Delta\omega^2} = \Delta_K / p_\nu$. The two scales $\overline{\Delta\omega^2} \leq \Delta_K$ determine the packet evolution details in the presence of nonlinearity.

The squared frequency shift of a single-site oscillator induced by the nonlinearity is $\delta_l \approx (3E_l)/(2\tilde{\epsilon}_l)$, where E_l is the energy of the oscillator. If instead a single mode is excited, its frequency shift is given by $\delta_\nu \approx (3E_\nu)/(2p_\nu \omega_\nu^2)$, with E_ν being the energy of the mode.

For small amplitudes the equations of motion of the KG chain can be approximately mapped onto a corresponding DNLS model [17]. In our notation, the mapping takes the following form. For the KG model with given parameters W and E, the corresponding DNLS model (1) with norm $S=1$, has a nonlinearity parameter $\beta \approx 3WE$. The norm density of the DNLS model corresponds to the normalized energy density of the KG model.

C. Computational methods

We will present results on long time numerical simulations. We therefore first discuss the methods and particularities of our computations. For both models, we used symplectic integrators. These integration schemes replace the original Hamiltonian by a slightly different one, which is integrated exactly. The smaller the time steps, the closer both Hamiltonians. Therefore, the computed energy (or norm) of the original Hamiltonian function will fluctuate in time but not grow. The fluctuations are bounded and are due to the fact that the actual Hamiltonian, which is integrated, has slightly different energy.

Another possible source of errors is the round-off procedure of the actual processor when performing operations with numbers. Sometimes it is referred to as "computational noise" although it is exactly the opposite, i.e., purely deterministic and reproducible. We will discuss the influence of round-off errors on our results in Sec. III F.

The KG chain was integrated with the help of a symplectic integrator of order $\mathcal{O}(\tau^4)$ with respect to the integration time step τ, namely, the $SABA_2$ integrator with corrector ($SABA_2C$), introduced in [18]. A brief presentation of the integration scheme, as well as its implementation for the particular case of the KG lattice [Eq. (6)] is given in the Appendix. The $SABA_2C$ integration scheme proved to be very efficient for long integrations (e. g. up to 10^{10} time units) of lattices having typically $N=1000$ sites (see, for example, the right plots of Fig. 2) since it kept the required computational time to feasible levels, preserving at the same time quite well the energy of the system. For example, an integration time step $\tau=0.2$ usually kept the relative error of the energy smaller than 10^{-4}.

The DNLS chain was integrated with the help of the $SBAB_2$ integrator (see the Appendix), which introduces an error in energy conservation of the order $\mathcal{O}(\tau^2)$. The number of sites used in our computations varied from $N=500$ to $N=2000$, in order to exclude finite-size effects in the evolution of the wave packets. For $\tau=0.1$ the relative error of energy was usually kept smaller than 10^{-3}. It is worth mentioning that, although the $SBAB_2$ integrator and the commonly used leap-frog integrator introduce errors of the same order, the $SBAB_2$ scheme exhibits a better performance since it requires less CPU time, keeping at the same time the relative energy error to smaller values than the leap-frog scheme.

We order the NMs in space by increasing value of the center-of-norm coordinate $X_\nu = \Sigma_l l A_{\nu,l}^2$. We analyze normalized distributions $z_\nu \geq 0$ using the second moment $m_2 = \Sigma_\nu (\nu - \bar{\nu})^2 z_\nu$, which quantifies the wave packet's degree of spreading and the participation number $P = 1/\Sigma_\nu z_\nu^2$, which measures the number of the strongest excited sites in z_ν. Here $\bar{\nu} = \Sigma_\nu \nu z_\nu$. For DNLS we follow norm density distributions

$z_\nu \equiv |\phi_\nu|^2/\Sigma_\mu |\phi_\mu|^2$. For KG we follow normalized energy density distributions $z_\nu \equiv E_\nu/\Sigma_\mu E_\mu$ with $E_\nu = \dot{A}_\nu^2/2 + \omega_\nu^2 A_\nu^2/2$, where A_ν is the amplitude of the νth NM and $\omega_\nu^2 = 1 + (\lambda_\nu + 2)/W$.

III. WAVE PACKET EVOLUTION

Below we will mainly use the DNLS case for theoretical considerations and also discuss crucial points to be taken into account when considering the KG case. We will present numerical results for both models.

We first consider a wave packet at $t=0$ which is compact either in real space or in normal-mode space. Compactness in real space implies a single-site excitation $\psi_l = \delta_{l,l_0}$ with the choice $\epsilon_{l_0} = 0$ for the DNLS model. For the KG model we set $p_l = 0$ and $u_l = c\delta_{l,l_0}$, with $\tilde{\epsilon}_{l_0} = 1$ and c being a constant which defines the initial energy E. Compactness in normal-mode space instead implies a single-mode excitation $\phi_\nu = \delta_{\nu,\nu_0}$ with $\lambda_{\nu_0} \approx 0$ for the DNLS model, while in the case of the KG system we have $A_\nu = c\delta_{\nu,\nu_0}$ and $\dot{A}_\nu = 0$, with $\omega_{\nu_0}^2 \approx 1 + (2/W)$, i.e., $\omega_{\nu_0}^2$ is located in the middle of the frequency spectrum. Again the constant c defines the initial energy of the wave packet. We will later also consider finite-size initial distributions of width L.

A. Expected regimes

Let us consider a single-site initial excitation with a corresponding nonlinear frequency shift δ_l. We compare this frequency shift with the two scales set by the linear equations: the average spacing $\overline{\Delta\lambda}$ (which corresponds to $\overline{\Delta\lambda}_D$ for DNLS and to $\overline{\Delta\omega^2}$ for KG) and the spectrum width Δ (with Δ denoting Δ_D for DNLS and Δ_K for KG). We expect three qualitatively different dynamical regimes: (I) $\delta_l < \overline{\Delta\lambda}$, (II) $\overline{\Delta\lambda} < \delta_l < \Delta$, and (III) $\Delta < \delta_l$. In case I the local frequency shift is less than the average spacing between interacting modes; therefore no initial resonance overlap of them is expected, and the dynamics may (at least for long times) evolve as in the linear case ($\beta=0$ for DNLS and $E \to 0$ for KG). In case II resonance overlap may happen immediately, and the packet should evolve differently. For case III the frequency shift exceeds the spectrum width; therefore some renormalized frequencies of NMs (or sites) may be tuned out of resonance with the NM spectrum, leading to self-trapping. The above definitions are highly qualitative since localized initial conditions are subject to strong fluctuations.

If we instead consider a single-mode initial excitation, we have to replace δ_l by δ_ν in the above argumentation. For both the DNLS and the KG model, it follows $\delta_l \sim p_\nu \delta_\nu$. The mean NM participation number (the localization volume) $p_\nu > 1$ depends on the disorder strength W.

If an initial excitation of the DNLS model is characterized by some exponentially localized (not necessarily compact) distribution ψ_l with $S=1$, the nonlinear frequency shift may be roughly estimated as $\delta \sim \beta |\psi|^2$, where the maximum norm density $|\psi|^2 = \sup_l |\psi_l|^2$. The left graph of Fig. 1 shows the location of the three different regimes in the plane of the control parameters, i.e., the frequency shift δ and the disorder strength W. Note that $\overline{\Delta\lambda} \propto W^3$ for $W \ll 1$ [15], and the intermediate regime II disappears around $W \approx 20$, where the participation number of a NM becomes of the order of 1, and the NMs become almost single-site solutions. Similarly, for the KG model we have the estimation $\delta \sim E$ and the corresponding parameter space of the three different regimes is shown in the right graph of Fig. 1.

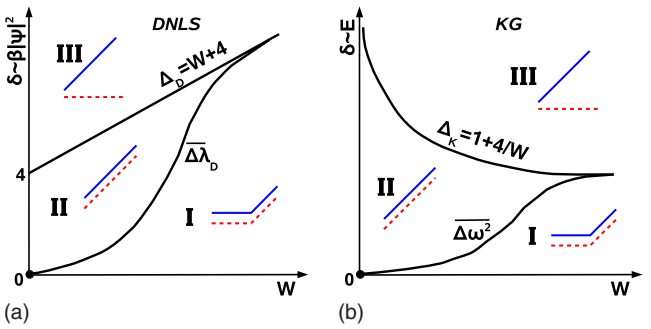

FIG. 1. (Color online) Schematic representations of the three different regimes of spreading for the DNLS (left graph) and the KG model (right graph) in the parameter space of disorder strength W and of the nonlinear frequency shift δ at initial time $t=0$. For each regime the dependence of $\log m_2$ (blue solid curves) and of $\log P$ (red dashed curves) versus $\log t$ are shown schematically (see section III C for details).

B. Self-trapping theorem

Regime III is also captured by a theorem presented in [10], which proves that for $\beta > \Delta$ (for the DNLS case) the single-site excitation can not uniformly spread over the entire (infinite) lattice. Indeed, with the notations

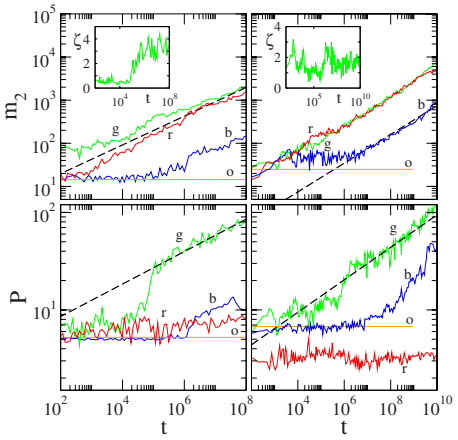

FIG. 2. (Color online) Single-site excitations. m_2 and P versus time in log-log plots. Left plots: DNLS with $W=4$, $\beta = 0, 0.1, 1, 4.5$ [(o), orange; (b), blue; (g) green; and (r) red]. Right plots: KG with $W=4$ and initial energy $E = 0.05, 0.4, 1.5$ [(b) blue; (g) green; and (r) red]. The orange (o) curves correspond to the solution of the linear equations of motion, where the term u_l^3 in Eq. (7) was absent. The disorder realization is kept unchanged for each of the models. Dashed straight lines guide the eyes for exponents $1/3 (m_2)$ and $1/6 (P)$, respectively. Insets: the compactness index ζ as a function of time in linear–log plots for $\beta=1$ (DNLS) and $E=0.4$ (KG).

$$\mathcal{H}_D = \mathcal{H}_{NL} + \mathcal{H}_L, \tag{8}$$

$$\mathcal{H}_L = \sum_l \epsilon_l |\psi_l|^2 - (\psi_{l+1}\psi_l^* + \psi_{l+1}^*\psi_l), \tag{9}$$

$$\mathcal{H}_{NL} = \sum_l \frac{\beta}{2}|\psi_l|^4 \equiv \frac{\beta}{2}P_r^{-1}, \tag{10}$$

where P_r is the participation number in real space, the single-site excitation at time $t=0$ yields

$$\mathcal{H}_L(t=0) = 0, \quad \mathcal{H}_{NL}(t=0) = \frac{\beta}{2}. \tag{11}$$

Due to norm conservation $S=1$ at all times, the harmonic energy part $\mathcal{H}_L$ is bounded from above and below [10]:

$$-2 - \frac{W}{2} \leq \mathcal{H}_L \leq 2 + \frac{W}{2}. \tag{12}$$

Due to energy conservation, for all times the anharmonic energy part $\mathcal{H}_{NL}$ can therefore not become smaller than

$$\mathcal{H}_{NL}(t) \geq \frac{\beta}{2} - 2 - \frac{W}{2}. \tag{13}$$

It follows with Eq. (10) that the participation number is bounded from above by a finite number, which diverges for $\beta=\Delta$:

$$P_r(t) \leq \frac{\beta}{\beta - \Delta} \quad \text{if} \quad \beta \geq \Delta \quad . \tag{14}$$

Moreover, since $P_r^{-1} = \Sigma_l |\psi_l|^4 < \sup_l |\psi_l|^2$ [10], we conclude that

$$\sup_l |\psi_l|^2(t) > \frac{\beta - \Delta}{\beta}. \tag{15}$$

Therefore, at least a part of the wave packet will not spread and will stay localized although the theorem does not prove that the location of that inhomogeneity is constant in time. The norm of the part of the wave packet, which can spread uniformly over the entire system, is bounded from above by $S_\infty \leq \Delta/\beta$.

C. Numerical results

We first show results for single-site excitations [11]. We systematically studied the evolution of wave packets for lattices (1) and (6). The scenario described in Sec. III A was observed very clearly. Representative examples are shown in Fig. 2. Regime III yields self-trapping (see also Figs. 1 and 3 in [10]), therefore P does not grow significantly, while the second moment $m_2 \sim t^\alpha$ with $\alpha \approx 1/3$ (red curves). Thus a part of the excitation stays highly localized [10], while another part delocalizes. Regime II yields subdiffusive spreading with $m_2 \sim t^\alpha$ and $P \sim t^{\alpha/2}$ [7,8] (green curves). Regime I shows the Anderson localization up to some time τ_d which increases with decreasing nonlinearity. For $t < \tau_d$ both m_2 and P are not changing. However for $t > \tau_d$ a detrapping takes place, and the packet starts to grow with characteristics as in regime II (blue curves). The simulation of the equations of motion in the absence of nonlinear terms (orange curves) demonstrates the appearance of the Anderson localization.

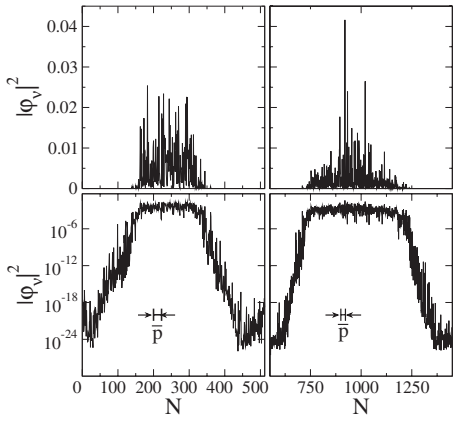

FIG. 3. Norm density distributions in the NM space at time $t = 10^8$ for the initial excitations in the regime II of the DNLS model shown in the left plots of Figs. 2 and 5. Left plots: single-site excitation for $W=4$ and $\beta=1$. Right plots: single-mode excitation for $W=4$ and $\beta=5$. $|\phi_\nu|^2$ is plotted in linear (logarithmic) scale in the upper (lower) plots. The maximal mean value of the localization volume of the NMs $\bar{p} \approx 22$ (shown schematically in the lower plots) is much smaller than the length over which the wave packets have spread.

The second moment m_2 is sensitive to the spreading distance of the tails of a distribution, while the participation number P is a measure of the inhomogeneity of the distribution, being insensitive to any spatial correlations. Thus, P and m_2 can be used to quantify the sparseness of a wave packet. To this end, we introduce as a measure of the compactness of a wave packet the compactness index

$$\zeta = \frac{P^2}{m_2}. \tag{16}$$

Let us consider a wave packet of K sites ($K \gg 1$). In the case where all the K sites are equally excited the compactness index is given by $\zeta=12$. In the case of a symmetric wave packet formed by a sequence of an excited site followed by a nonexcited one, where all the $K/2$ excited sites have the same amplitude, $\zeta=3$. Distributions with larger gaps between the equally excited isolated sites attain a compactness index $\zeta<3$. For the extreme case of a sparse wave packet formed by two equally excited sites located at the two edges of the packet, i.e., when only sites 1 and K($K \gg 1$) are excited to an amplitude 1/2, the compactness index is $\zeta = 16/K^2$. So, smaller values of ζ correspond to more sparse wave packets.

We expect that ζ in regime I will remain constant for $t < \tau_d$ and will behave as in the case of regime II for later times. In regime II ζ would either be constant or decay in time, while in regime III it should decay since P remains practically constant. The time evolution of ζ for excitations in regime II is shown in the insets of Fig. 2. As one can see the compactness index oscillates around some constant non-

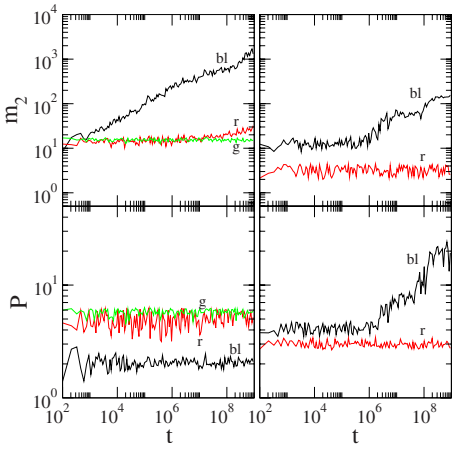

FIG. 4. (Color online) Single-site excitations for the same disorder realization of the KG model. m_2 and P versus time in log–log plots. Left panels: plots for $W=4$ and initial energy $E=3.225,4,10$ [(bl) black, (r) red, and (g) green]. Right panels: Plots for $E=0.05$ and $W=6,7$ [(bl) black and (r) red].

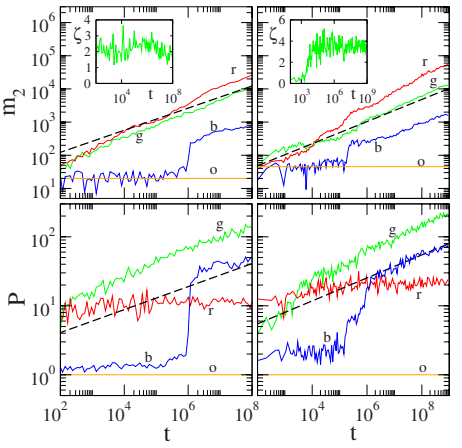

FIG. 5. (Color online) Single-mode excitations. m_2 and P versus time in log–log plots. Left plots: DNLS with $W=4$, $\beta=0,0.6,5,30$ [(o) orange, (b) blue, (g) green, and (r) red]. Right plots: KG with $W=4$ and initial energy $E=0.17,1.1,13.4$ [(b) blue, (g) green, and (r) red]. The orange curves (o) correspond to the solution of the linear equations of motion, where the term u_l^3 in Eq. (7) was absent. The disorder realization is kept unchanged for each of the models. Dashed straight lines guide the eye for exponents $1/3(m_2)$ and $1/6(P)$, respectively. Insets: the compactness index ζ as a function of time in linear–log plots for $\beta=5$ (DNLS) and $E=1.1$ (KG).

zero value both for the DNLS and the KG models. This means that the wave packet spreads but does not become more sparse. For the particular cases of Fig. 2 the compactness index attains the values $\zeta=3.5$ for the DNLS model at $t=10^8$ and $\zeta=1.7$ for the KG chain at $t=10^{10}$. The corresponding wave packet of the DNLS model is shown in the left plots of Fig. 3.

Partial nonlinear localization in regime III is explained by self-trapping [10]. It is due to tuning frequencies of excitations out of resonance with the NM spectrum, takes place irrespective of the presence of disorder, and is related to the presence of exact t-periodic spatially localized states (also coined discrete breathers) for ordered [19] and disordered systems [20] (in the latter case also t-quasiperiodic states exist). These exact solutions act as trapping centers.

Note that for large nonlinearities ($\beta \gg \Delta$ for DNLS or large energy values E of the KG model) almost the whole excitation is self-trapped. This behavior can be seen in the left plots of Fig. 4, where the time evolution of m_2 and P for different values of the energy E of the KG chain is shown. The value of W is kept to $W=4$ as in the cases presented in the right plots of Fig. 2. As the energy increases the portion of the wave packet that stays self-trapped increases with respect to the part that diffuses. Thus, we observe a change in the evolution of m_2 from subdiffusive increase to practical constancy. On the other hand, P is not affected as it continues to fluctuate around some constant value.

The Anderson localization on finite times in regime I is observed on potentially large time scales τ_d, and as in regime III, regular states act as trapping centers [20]. For $t > \tau_d$, the wave packet trajectory finally departs away from the vicinity of regular orbits with subsequent spreading. Increasing the value of W results to small localization lengths of NMs and thus, the Anderson localization will persist for extremely long time intervals. Since our numerical computations are limited in time, we are not able to observe the detrapping phase of the evolution when W increases significantly. This behavior can be seen in the right plots of Fig. 4 where we consider initial single-site excitations which, for $W=4$ (see right plots of Fig. 2), belong to regime I. In these plots we observe a direct transition from regime I to practical constancy of m_2 and P as W increases, at least up to the final integration time used.

For single-mode excitations we find a similar outcome but with rescaled critical values for the nonlinearity strength which separate the different regimes. Examples of the three different regimes are shown in Fig. 5. As in the case of single-site excitations presented in Fig. 2, the compactness index ζ plotted in the insets if Fig. 5 remains practically constant for excitations in regime II, attaining the values $\zeta=1.5$ at $t=10^8$ for the DNLS model and $\zeta=3.3$ at $t=10^9$ for the KG chain. The final norm density distribution for the DNLS model is plotted in the right plots of Fig. 3. The average value $\bar{\zeta}$ of the compactness index over 20 realizations at $t=10^8$ for the DNLS model with $W=4$ and $\beta=5$ was found to be $\bar{\zeta}=2.95\pm0.39$.

D. Spreading

The subdiffusive spreading takes place in regime I for $t > \tau_d$, in regime II, and for a part of the wave packet also in regime III. For single-site excitations the exponent α does not appear to depend on β in the case of the DNLS model or on the value of E in the case of KG. In Fig. 6 we show results for $m_2(t)$ in regime II for different values of the disorder strength W. Again we find no visible dependence of the exponent α on W. Therefore the subdiffusive spreading is rather universal and the parameters β (or E) and W are only affecting the prefactor. Excluding self-trapping, any nonzero nonlinearity will completely delocalize the wave packet and

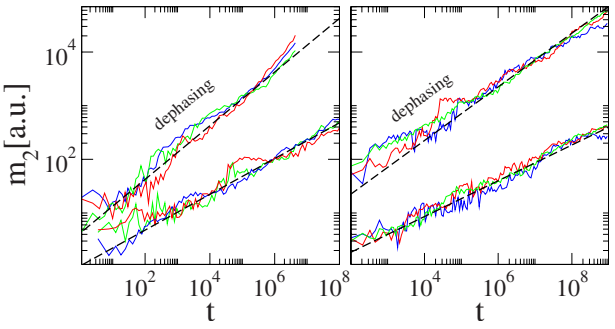

FIG. 6. (Color online) Single-site excitations. m_2 (in arbitrary units) versus time in log-log plots in regime II and different values of W. Lower set of curves: plain integration (without dephasing); upper set of curves: integration with dephasing of NMs (see Sec. IV A). Dashed straight lines with exponents 1/3 (no dephasing) and 1/2 (dephasing) guide the eye. Left plot: DNLS, $W=4$ and $\beta=3$ (blue); $W=7$ and $\beta=4$ (green); $W=10$ and $\beta=6$ (red). Right plot: KG, $W=10$ and $E=0.25$ (blue); $W=7$ and $E=0.3$ (red); $W=4$ and $E=0.4$ (green). The curves are shifted vertically in order to give maximum overlap within each group.

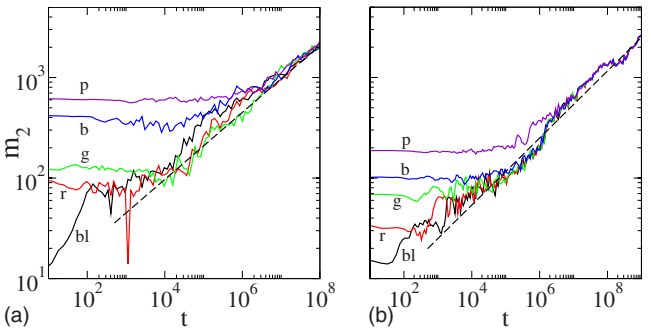

FIG. 7. (Color online) Evolution of m_2 versus time in log-log plots. Single-site excitations in the intermediate regime II for the DNLS (a) and the KG model (b) correspond to black curves (bl). The wave packets after $t_d=10^3$, 10^4, 10^5, and 10^6 time units (t.u.) [(r) red; (g) green; (b) blue; and (p) purple] are registered and relaunched as initial distributions (colored curves). The dashed straight lines correspond to functions $\propto t^{1/3}$.

destroy the Anderson localization. We performed fittings by analyzing 20 runs in regime II with different disorder realizations. For each realization we fitted the exponent α and then averaged over all computational measurements. We find $\alpha=0.33\pm0.02$ for DNLS, and $\alpha=0.33\pm0.05$ for KG. Therefore, the predicted universal exponent $\alpha=1/3$ [11] appears to explain the data.

On the other hand, in the case of single-mode excitations the numerically computed values of the exponent α seem to be slightly larger than $\alpha=1/3$, as can be also seen from the results of Fig. 5. In particular, m_2 in regimes II and III of the DNLS model and in regime III of the KG model increases slightly faster than $\propto t^{1/3}$, which is represented by the dashed lines in the upper plots of Fig. 5. In addition, the value of the exponent seems to slightly vary with respect to the nonlinearity parameter β for DNLS and E for KG. The reason of the slightly different behavior between single-site and single-mode excitations is still an open issue.

E. Detrapping

In the intermediate regime II the wave packet starts to spread almost from scratch. We do not observe any saturation and crossover into localization on later times. Let us assume that the wave packet spreads without limitations. The initial nonlinear frequency shift δ_l was larger than the average level spacing in a localization volume $\Delta\lambda$. However, δ_l will become smaller than $\Delta\lambda$ at some later time since $\sup_l|\psi_l|^2$ ($\sup_l E_l$ for KG) decreases in time as the wave packet spreads. Therefore, there will be a large but finite time t_d, at which we cross over from the intermediate regime II into the weak nonlinearity regime I. The arresting of the wave packet up to a time τ_d in the weak nonlinearity regime I can be explained by a correspondingly large spreading time scale τ_d. For $t<\tau_d$ no spreading is observed when monitoring the second moment m_2, with subsequent spreading observed on larger time scales $t>\tau_d$.

We test the above conclusions by the following simple scheme. We start a single-site excitation in the intermediate regime II, measure the distribution at some time t_d, and relaunch the distribution as an initial condition at time $t=0$. The results are shown in Fig. 7. We find that the relaunched runs yield a second moment m_2 which appears to be constant up to the time $\tau_d\approx t_d$ with a subsequent spreading, similar to the previously obtained detrapping in regime I.

For a specific value of the nonlinearity β of the DNLS model let each NM in the packet after some spreading to have norm $|\phi_\nu|^2\sim n\ll 1$, with n denoting the average norm density of the excited NMs (in the case of the KG model n corresponds to the average energy density of the excited NMs). The packet size is then $1/n\gg\bar{p}$, with $\bar{p}=\max_\nu p_\nu$, and the second moment $m_2\sim 1/n^2$. Let us assume that the second moment grows as $m_2\sim t^{1/3}$. Let us also assume that at any time the spreading is due to some diffusion process and is characterized by some momentary diffusion rate $D(t)$ such that $m_2=D(t)t$. Then it follows that $D(t)\sim t^{-2/3}$ and finally $D\sim n^4$. Such a result has to be the outcome of the action of the nonlinear terms (which always contain products βn). A diffusion rate is equal to an inverse characteristic time scale, and therefore we conjecture

$$D=\tau_d^{-1}\sim\beta^4 n^4. \tag{17}$$

There are two ways of modifying D. We can either spread our initial excitation over some number of sites L, therefore varying n. Alternatively we can fix the shape of the initial excitation and vary β.

In order to test the validity of Eq. (17) for a fixed value of nonlinearity we considered a single-site excitation in the intermediate regime II for the KG model with total energy $E=0.4$ so that m_2 and P start to grow from the beginning [black curves in Figs. 8(a) and 8(b), respectively]. We also followed the time evolution of wave packets having as initial condition a homogeneous distribution of the energy $E=0.4$ among L neighboring sites. In particular, we considered initial distributions with $u_l=0$ and $p_l=0$ except for the central L sites whose initial momenta were set to $\pm\sqrt{2E/L}$, with the

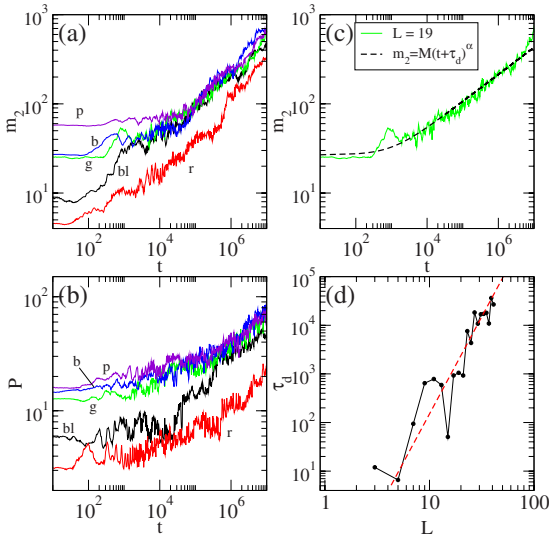

FIG. 8. (Color online) Nonlocal excitations of the KG chain corresponding to initial homogeneous distributions of energy $E=0.4$ over L neighboring sites. (a) m_2 and (b) P versus time in log-log plots for $L=1$, 9, 19, 29, and 39 sites [(bl) black; (r) red; (g) green; (b) blue; and (p) purple]. (c) Fitting of the time evolution of m_2 for $L=19$ with a curve of the form (18) for $M=3.25$, $\tau_d=1052$, and $\alpha=0.303$. (d) The dependence of the detrapping time τ_d on the number L of initially excited sites in log-log scale. The dashed straight line corresponds to a function $\propto L^4$.

sign changing randomly from site to site. We performed simulations with L ranging from 1 up to 41. The time evolution of m_2 and P for some of these cases is shown in Figs. 8(a) and 8(b), respectively. In accordance to the results presented in Fig. 7 we observe that distributing the energy of a single-site excitation belonging to regime II over more sites results in a time dependence of m_2 and P similar to regime I, i.e., both quantities start to increase after some transient detrapping time τ_d.

The behavior of the second moment $m_2(t)$ can be modeled by a function of the form

$$m_2(t) = M(t + \tau_d)^{\alpha}, \tag{18}$$

where M is a constant related to the value of the second moment of the initial distribution $m_2(0)=M\tau_d^{\alpha}$. Equation (18) gives a power-law dependence of m_2 on t for $t \gg \tau_d$ and a slow time dependence of m_2 for $t \ll \tau_d$. Thus, it can be used to describe the behavior of m_2 for $L>1$. Fitting the numerical data obtained for different values of L by Eq. (18) [see Fig. 8(c) for such an example], we can determine the dependence of τ_d on L [Fig. 8(d)]. Since $L \sim n^{-1}$ from Eq. (17) we conclude that $\tau_d \sim L^4$. As we can see from Fig. 8(d) the numerically obtained results are in good agreement with this assumption.

To test the dependence of D on β, we studied the weak nonlinearity regime I for the DNLS model with $W=4$. We launched single-site excitations for ten realizations for $\beta=0.1$ and $\beta=0.2$. We estimated the detrapping times τ_d on logarithmic scale for each run and averaged over each group of realizations. As a result we obtain $\langle \log_{10} \tau_d \rangle = 5$ for $\beta=0.2$, and $\langle \log_{10} \tau_d \rangle = 6.9$ for $\beta=0.1$ (with $\langle \cdots \rangle$ denoting the mean value over the realizations), and their difference is then 1.9. According to Eq. (17), the difference should be 1.2 which is in relatively good agreement with the numerically estimated value.

F. Numerical accuracy and round-off errors

We performed several tests in order to ensure that our results are not generated by inaccurate computations. First we varied the size of the system and found no dependence of the results on it. Therefore we exclude finite-size effects.

Second we varied the time steps of the symplectic integration schemes by orders of magnitudes. Again we found no visible change in the detrapping times or in the spreading characteristics. We also used different integration schemes and even nonsymplectic ones (eighth-order Runge-Kutta). No changes were obtained either. Therefore we exclude effects due to discretization of time.

Finally we studied the influence of computational round-off errors. The above observation, in which the variation in time steps does not change the key results, implicitly tells that round-off errors can be excluded as well. Indeed, changing the time steps, we change the number of operations to be performed on a given interval of integration. Therefore we change the number of round-off operations.

In addition, we decided to perform further tests with respect to the round-off error issue. These tests are inspired by the following consideration. Floating point numbers are characterized by the number of digits a after the comma which are kept during computations. All presented data were obtained with double precision, where $a=16$. The detrapping and spreading can be only due to the cubic nonlinear terms in the equations of motion. These terms are added to linear terms, when calculating the right-hand side of Eqs. (2) and (7). Therefore, when for example in the case of the DNLS model $\sup_l |\psi_l|^2 < 10^{-8}$, the nonlinear terms become of the order of the round-off error of the linear terms. For all of our simulations, the amplitudes in the packet are of the order of 10^{-2} or larger. Therefore the roundoff is affecting only the amplitudes far in the exponential tails. We changed the calculation to single precision, for which $a=8$, but we did not observe any qualitative difference in our results. For single precision the nonlinear terms will be affected by round-off errors when $\sup_l |\psi_l|^2 < 10^{-4}$, which is still realized only in the exponential tails. We note that the times at which the round-off errors affect the packet modes correspond to $t \sim 10^{80}$ for $a=16$ and $t \sim 10^{30}$ for $a=8$ which are obviously not accessible with our computation schemes.

Therefore we implemented a brute force round-off scheme: after each time step of integration we take the distributions and perform a roundoff at a prescribed digit $a=1,2,3,4,\ldots$. We expect therefore to reduce the time at which round-off errors will become visible in order to observe that effect within the time window accessible by our computations. Indeed, we find that strong fluctuations in the conserved quantities set in at a time t_r which decreases with decreasing a. In particular for the DNLS we find $t_r \approx 10^3, 10^5, 10^7$ for $a=1,2,3$, and for the KG model we find $t_r \approx 10^3, 10^5, 10^8$ for $a=1,2,3$. When monitoring the second

moment and the participation number, we also find strong deviations from the above results at times $t > t_r$. For $a \geq 4$ we do not observe any significant change in the data. Therefore we conclude, that the round-off errors with double (or even single) precision are not affecting our results.

IV. SPREADING MECHANISMS

We can think of two possible mechanisms of wave packet spreading. A NM with index μ in a layer of width $\bar{p}$ in the cold exterior, which borders the packet, is either incoherently *heated* by the packet or *resonantly excited* by some particular NM from a layer with width $\bar{p}$ inside the packet. Heating here implies a (sub)diffusive spreading of energy. Note that the numerical results yield subdiffusion, supporting the nonballistic diffusive heating mechanism.

For heating to work, the packet modes $\phi_\nu(t)$ should contain a part $\phi_\nu^c(t)$, having a continuous frequency spectrum (similar to a white noise), in addition to a regular part $\phi_\nu^r(t)$ of pure point frequency spectrum:

$$\phi_\nu(t) = \phi_\nu^r(t) + \phi_\nu^c(t). \tag{19}$$

Therefore at least some NMs of the packet should evolve chaotically in time. The more the packet spreads, the less the mode amplitudes in the packet become. Therefore its dynamics should become more and more regular, implying $\lim_{t\to\infty} \phi_\nu^c(t)/\phi_\nu^r(t) \to 0$.

A. Are all packet modes chaotic?

In Ref. [8] it was assumed that all NMs in the packet are chaotic, and their phases can be assumed to be random at all times. At variance to the above expectation, it follows that $\phi_\nu^r(t)=0$ or at least the ratio $\phi_\nu^c(t)/\phi_\nu^r(t)$ is constant on average. Consequently $|\phi_\nu^c(t)| \sim n^{1/2}$, where n is the average norm density in the packet.

According to Eq. (4) the heating of the exterior mode should evolve as $i\dot{\phi}_\mu \approx \lambda_\mu \phi_\mu + \beta n^{3/2} f(t)$ where $\langle f(t) f(t') \rangle = \delta(t-t')$ ensures that $f(t)$ has a continuous frequency spectrum. Then the exterior NM increases its norm according to $|\phi_\mu|^2 \sim \beta^2 n^3 t$. The momentary diffusion rate of the packet is given by the inverse time T it needs to heat the exterior mode up to the packet level: $D = 1/T \sim \beta^2 n^2$. The diffusion equation $m_2 \sim Dt$ yields $m_2 \sim \beta t^{1/2}$. We tested the above conclusions by enforcing decoherence of NM phases. Each 100 time units on average 50% of the NMs were randomly chosen, and their phases were shifted by π (DNLS). For the KG case we changed the signs of the corresponding NM momenta. We obtain $m_2 \sim t^{1/2}$ (see Fig. 6). Therefore, when the NMs dephase completely, the exponent $\tilde{\alpha} = 1/2$, *contradicting* numerical observations *without dephasing*. Thus, not all NMs in the packet are chaotic, and dephasing is at best a partial outcome.

B. Mode-mode resonances inside the packet

Chaos is a combined result of resonances and nonintegrability. Let us estimate the number of resonant modes in the packet for the DNLS model. Excluding secular interactions, the amplitude of a NM with $|\phi_\nu|^2 = n_\nu$ is modified by a triplet of other modes $\vec{\mu} \equiv (\mu_1, \mu_2, \mu_3)$ in first order in β as Eq. (4);

$$|\phi_\nu^{(1)}| = \beta \sqrt{n_{\mu_1} n_{\mu_2} n_{\mu_3}} R_{\nu,\vec{\mu}}^{-1}, \quad R_{\nu,\vec{\mu}} \sim \left| \frac{\vec{d\lambda}}{I_{\nu,\mu_1,\mu_2,\mu_3}} \right|, \tag{20}$$

where $\vec{d\lambda} = \lambda_\nu + \lambda_{\mu_1} - \lambda_{\mu_2} - \lambda_{\mu_3}$. The perturbation approach breaks down and resonances set in when $\sqrt{n_\nu} < |\phi_\nu^{(1)}|$. Since all considered NMs belong to the packet, we assume their norms to be equal to n for what follows. If three of the four mode indices are identical, one is left with interacting NM pairs. A statistical analysis of the probability of resonant interaction was performed in Ref. [11]. For small values of n (i.e. when the packet has spread over many NMs) the main contribution to resonances are due to rare multipeak modes [11], with peak distances being larger than the localization volume. If two or none of the four mode indices are identical, one is left with triplets and quadruplets of interacting NMs, respectively. In both cases the resonance conditions can be met at arbitrarily small values of n for NMs from one localization volume.

We perform a statistical numerical analysis for the quadruplet case. For a given NM ν we obtain $R_{\nu,\vec{\mu}_0} = \min_{\vec{\mu}} R_{\nu,\vec{\mu}}$. Collecting $R_{\nu,\vec{\mu}_0}$ for many ν and many disorder realizations, we find the probability density distribution $\mathcal{W}(R_{\nu,\vec{\mu}_0})$ (Fig. 9). The main result is that $\mathcal{W}(R_{\nu,\vec{\mu}_0} \to 0) \to C(W) \neq 0$. For the cases studied, the constant C drops with increasing disorder strength W. Similar results are found if pairs of resonant NMs [11] are analyzed, with the only difference that the constant C is reduced, e.g., by a factor of 30 for $W=4$.

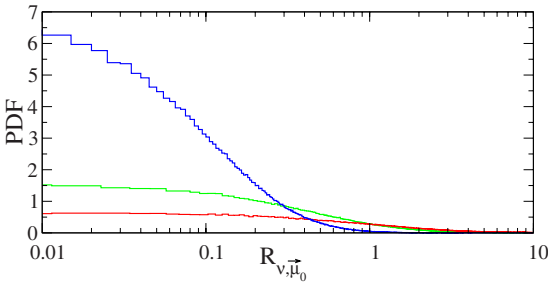

FIG. 9. (Color online) Statistical properties of NMs of the DNLS model. Probability densities $\mathcal{W}(R_{\nu,\vec{\mu}_0})$ of NMs being resonant (see Sec. IV B for details). Disorder strength $W=4, 7, 10$ (from top to bottom).

The probability $\mathcal{P}$ for a mode, which is excited to a norm n (the average norm density in the packet), to be resonant with at least one triplet of other modes at a given value of the interaction parameter β is given by

$$\mathcal{P} = \int_0^{\beta n} \mathcal{W}(x) dx, \tag{21}$$

with x denoting $R_{\nu,\vec{\mu}_0}$. For $\beta n \ll 1$ it follows

$$\mathcal{P} \approx C\beta n \quad . \tag{22}$$

Therefore the probability for a mode in the packet to be resonant is proportional to $C\beta n$. On average the number of resonant modes in the packet is constant, proportional to $C\beta$, and their fraction within the packet is $\sim C\beta n$. Since packet mode amplitudes fluctuate in general, averaging is meant both over the packet and over suitably long time windows (yet short compared to the momentary inverse packet growth rate). We conclude that the continuous frequency part of the dynamics of a packet mode is scaled down by $C\beta n$ compared to the case when all NMs would be chaotic. It follows that $\phi_\nu^c(t)/\phi_\nu^r(t) \sim C\beta n$. As expected initially, the chaotic part in the dynamics of packet modes becomes weaker the more the packet spreads, and the packet dynamics becomes more and more regular in the limit of large times. Therefore the chaotic component $\phi_\nu^c(t) \ll \phi_\nu^r(t)$ is a small parameter.

Expanding the term $|\phi_\nu|^2\phi_\nu$ to first order in $\phi_\nu^c(t)$, the heating of the exterior mode should evolve according to $i\dot{\phi}_\mu \approx \lambda_\mu \phi_\mu + C\beta^2 n^{5/2} f(t)$. It follows $|\phi_\mu|^2 \sim C^2\beta^4 n^5 t$, and the rate $D=1/T \sim C^2\beta^4 n^4$ [cf. prediction (17)]. The diffusion equation $m_2 \sim Dt$ yields

$$m_2 \sim C^{2/3}\beta^{4/3} t^\alpha, \quad \alpha = 1/3. \tag{23}$$

The predicted exponent $\alpha=1/3$ is close to the numerically observed one, as we discussed in Sec. III D.

C. Resonant spreading?

Finally we consider the process of resonant excitation of an exterior mode by a mode from the packet. The number of packet modes in a layer of the width of the localization volume at the edge, which are resonant with a cold exterior mode, will be proportional to βn. After long enough spreading $\beta n \ll 1$. On average there will be no mode inside the packet, which could efficiently resonate with an exterior mode. Therefore, resonant growth can be excluded.

V. SUMMARY AND DISCUSSION

We studied the spreading of wave packets in disordered one-dimensional nonlinear chains. In particular we considered two systems, namely, the DNLS model [Eq. (1)] and the quartic KG system [Eq. (6)]. The linear parts of these two models are equivalent in the sense that they correspond to the same eigenvalue problem [Eq. (3)].

We predicted theoretically and verified numerically the existence of three different dynamical behaviors depending on the relation of the nonlinear frequency shift δ (which is proportional to the system's nonlinearity) with the average spacing $\overline{\Delta\lambda}$ of eigenfrequencies and the spectrum width $\Delta(\overline{\Delta\lambda} \leq \Delta)$ of the linear system. The dynamics for small nonlinearities ($\delta < \overline{\Delta\lambda}$) is characterized by localization as a transient with subsequent subdiffusion (regime I). For intermediate values of the nonlinearity $\overline{\Delta\lambda} < \delta < \Delta$, and the wave packets exhibit immediate subdiffusion (regime II). In this case, the second moment m_2 and the participation number P increase in time following the power laws $m_2 \sim t^\alpha$ and $P \sim t^{\alpha/2}$. Assuming that the spreading is due to an incoherent excitation of the cold exterior induced by the chaotic behavior of the wave packet, we predicted $\alpha=1/3$. Finally, for even higher nonlinearities ($\delta > \Delta$) a large part of the wave packet is self-trapped, while the rest subdiffuses (regime III). In this case P remains practically constant, while $m_2 \sim t^\alpha$. The overall picture is schematically presented in Fig. 1 both for the DNLS and the KG model.

The compactness index $\zeta = P^2/m_2$, which measures the sparseness of wave packets, exhibits different behaviors for the three dynamical regimes. In particular, the behavior of ζ for wave packets in regime II imply that these wave packets spread but do not become more sparse.

For large values of the disorder strength W and/or strong nonlinearity the intermediate regime II effectively disappears, and the evolution will start either in regime I or in regime III. In regime I the detrapping times increase with further increase of W. In regime III the fraction of the wave packet which spreads decreases with increasing nonlinearity. Therefore, large values of W and/or nonlinearity will not allow for an observation of the destruction of the Anderson localization on time scales which are bounded from above by practical computational limitations.

The subdiffusive spreading is universal, i.e., the exponent α is independent of the nonlinearity's strength (β for the DNLS model and energy E for the KG one) and W, which are only affecting the prefactor in Eq. (23). Excluding self-trapping, any nonzero nonlinearity strength β will completely delocalize the wave packet and destroy the Anderson localization. The exponent α is determined solely by the degree of nonlinearity, which defines the type of overlap integral to be considered in Eq. (20), and by the stiffness of the spectrum $\{\lambda_\nu\}$. Our numerical computations confirmed the prediction $\alpha=1/3$ in the case of single-site and nonlocal homogeneous excitations. In the case of single-mode excitations the three different regimes were also detected. The numerically computed exponents α get slightly larger values than 1/3, exhibiting also a small dependence on the strength of nonlinearity. This discrepancy between the two cases in not clearly understood.

We studied the statistics of detrapping times τ_d for regime I. We provided numerical evidences for the validity of the conjectured dependence of τ_d on the nonlinearity strength and on the average norm density of the excited NMs given in Eq. (17). It is worth mentioning that distributing the energy of a single-site excitation belonging to regime II over more sites results in a time dependence of m_2 and P similar to regime I. In addition, considering as initial condition the profile of a single-site excitation in regime II at some later time t_d, we observe a dynamical evolution of the type of regime I where the detrapping time is $\tau_d \approx t_d$.

The spreading of the wave packet is due to weak but nonzero chaotic dynamics inside the packet. It is natural to expect such a dynamics since the considered systems are nonintegrable. If instead an integrable system is considered, the Anderson localization will not be destroyed. Indeed, consider a Hamiltonian in NM representation using actions J_ν and angles θ_ν as coordinates:

$$\mathcal{H}_{int} = \sum_{\nu} \lambda_{\nu} J_{\nu} + \beta \sum_{\nu_1,\nu_2,\nu_3,\nu_4} I_{\nu_1,\nu_2,\nu_3,\nu_4} \sqrt{J_{\nu_1} J_{\nu_1} J_{\nu_1} J_{\nu_1}}. \quad (24)$$

We assume that the set of eigenfrequencies $\{\lambda_\nu\}$ and the overlap integrals $I_{\nu_1,\nu_2,\nu_3,\nu_4}$ are identical with those describing the DNLS model Eqs. (4) and (5). The equations of motion $\dot{J}_\nu = -\partial \mathcal{H}_{int}/\partial \theta_\nu$ and $\dot{\theta}_\nu = \partial \mathcal{H}_{int}/\partial J_\nu$ yield $\dot{J}_\nu = 0$ since the integrable Hamiltonian (24) depends only on the actions. Therefore, any localized initial condition [e.g., $J_\nu(t=0) \propto \delta_{\nu,\nu_0}$] will stay localized, since actions of modes which are at large distances will never get excited. Thus, the observed spreading of wave packets, which we studied in detail in the present work, is entirely due to the nonintegrability of the considered models at variance to Eq. (24).

The more the wave packet spreads, the weaker the resonances become. Corresponding structures (chaotic layers) in phase space become thinner and thinner. Consider quantum many-body systems. Classical phase space structures which are finer than the action quantization induced grid become irrelevant. Therefore we may speculate that the wave packet will stop spreading for a quantum many-body system at some point for zero temperature but also for temperatures below some finite threshold. These expectations are very close to rigorous results for interacting fermions in disordered systems [21].

In our study we considered initial conditions exciting NMs whose eigenvalues are located close to the center of the frequency band. Thus, the evolution of the system does not significantly depend on the sign of nonlinearity. In contrast, when one excites eigenstates with frequencies near the band edges, a rather weak nonlinearity might lead either to self-trapping or to the weak nonlinear regime depending on the sign of nonlinearity. Such examples were presented in [4] where NMs close to the edges of the band exhibit different dynamical behaviors, i.e., one becomes more localized as the nonlinearity was switched on, while the other tends to delocalize. If a spatially continuous system is considered, then a proper choice of the sign of nonlinearity prohibits self-trapping (so-called defocusing nonlinearity, corresponding to repulsive two-body interactions). For such a case, regime III ceases to exist, and localization is expected to be destroyed irrespectively of the strength of nonlinearity.

ACKNOWLEDGMENTS

We thank B. L. Altshuler, S. Aubry, G. Kopidakis, and R. Schilling for useful discussions.

APPENDIX: THE SABA$_2$ AND SBAB$_2$ SYMPLECTIC INTEGRATORS

In [18] a family of symplectic integrators which involve only forward integration steps was proposed. These integrators were adapted for integrations of perturbed Hamiltonians of the form

$$H = A + \epsilon B, \quad (A1)$$

where both A and B are integrable and ϵ is a parameter. We briefly recall here their main properties focusing our attention on two particular members of the family of integrators presented in [18], namely, the SABA$_2$ and SBAB$_2$ integrators. These integrators have already proved to be very efficient for the numerical study of astronomical [18], as well as accelerator models [22].

Consider a Hamiltonian system of N degrees of freedom having a Hamiltonian $H(\vec{p},\vec{u})$, with $\vec{p}=(p_1,\ldots,p_N)$, $\vec{u}=(u_1,\ldots,u_N)$, where u_l and p_l, with $l=1,\ldots,N$, are the generalized coordinates and momenta, respectively. An orbit of this system is defined by a vector $\vec{x}(t)=(x_1(t),\ldots,x_{2N}(t))$, with $x_l=p_l$ and $x_{l+N}=u_l$, where $l=1,\ldots,N$. This orbit is a solution of Hamilton's equations of motion:

$$\frac{d\vec{p_l}}{dt} = -\frac{\partial H}{\partial \vec{u_l}}, \quad \frac{d\vec{u_l}}{dt} = \frac{\partial H}{\partial \vec{p_l}}, \quad l = 1,\ldots,N, \quad (A2)$$

where t is the independent variable, namely, the time. Defining the Poisson bracket of functions $f(\vec{p},\vec{u})$ and $g(\vec{p},\vec{u})$ by

$$\{f,g\} = \sum_{l=1}^{N} \left(\frac{\partial f}{\partial p_l}\frac{\partial g}{\partial u_l} - \frac{\partial f}{\partial u_l}\frac{\partial g}{\partial p_l} \right), \quad (A3)$$

the Hamilton's equations of motion take the form

$$\frac{d\vec{x}}{dt} = \{H,\vec{x}\} = L_H \vec{x}, \quad (A4)$$

where L_H is the differential operator defined by $L_\chi f = \{\chi, f\}$. The solution of Eq. (A4), for initial conditions $\vec{x}(0)=\vec{x}_0$, is formally written as

$$\vec{x}(t) = \sum_{n\geq 0} \frac{t^n}{n!} L_H^n \vec{x}_0 = e^{tL_H}\vec{x}_0. \quad (A5)$$

A symplectic scheme for integrating Eq. (A4) from time t to time $t+\tau$ consists of approximating, in a symplectic way, the operator $e^{\tau L_H} = e^{\tau(L_A+L_{\epsilon B})}$ by an integrator of j steps involving products of $e^{c_i \tau L_A}$ and $e^{d_i \tau L_{\epsilon B}}$, with $i=1,2,\ldots,j$, which are exact integrations over times $c_i\tau$ and $d_i\tau$ of the integrable Hamiltonians A and B. The constants c_i and d_i are chosen so that to increase the order of the remainder of this approximation.

For the SABA$_2$ integrator we get

$$\mathrm{SABA}_2 = e^{c_1 \tau L_A} e^{d_1 \tau L_{\epsilon B}} e^{c_2 \tau L_A} e^{d_1 \tau L_{\epsilon B}} e^{c_1 \tau L_A}, \quad (A6)$$

with $c_1 = \frac{1}{2}(1-\frac{1}{\sqrt{3}})$, $c_2 = \frac{1}{\sqrt{3}}$, and $d_1 = \frac{1}{2}$, while the SBAB$_2$ integrator is given by

$$\mathrm{SBAB}_2 = e^{d_1 \tau L_{\epsilon B}} e^{c_2 \tau L_A} e^{d_2 \tau L_{\epsilon B}} e^{c_2 \tau L_A} e^{d_1 \tau L_{\epsilon B}}, \quad (A7)$$

with $c_2 = \frac{1}{\sqrt{2}}$, $d_1 = \frac{1}{6}$, and $d_2 = \frac{2}{3}$. Using these integrators we are actually approximating the dynamical behavior of the real

Hamiltonian $A+\epsilon B$ by a Hamiltonian $\tilde{H}=A+\epsilon B+\mathcal{O}(\tau^4\epsilon+\tau^2\epsilon^2)$, i.e., we introduce an error term of the order $\tau^4\epsilon+\tau^2\epsilon^2$.

The accuracy of the $SABA_2$ (or $SBAB_2$) integrator can be improved when the term $C=\{\{A,B\},B\}$ leads to an integrable system, as in the common situation of A being quadratic in momenta $\vec{p}$ and B depending only on positions $\vec{u}$. In this case, two corrector terms of small backward steps can be added to the integrator $SABA_2$,

$$\mathrm{SABA_2C} = e^{-(\tau^3\epsilon^2 g/2)L_C}(\mathrm{SABA_2})e^{-(\tau^3\epsilon^2 g/2)L_C}. \quad \text{(A8)}$$

A similar expression is valid also for $SBAB_2$. The value of g was chosen in order to eliminate the $\tau^2\epsilon^2$ dependence of the remainder which becomes of order $\mathcal{O}(\tau^4\epsilon+\tau^4\epsilon^2)$. In particular we have $g=(2-\sqrt{3})/2$ for $SABA_2$ and $g=\frac{1}{72}$ for $SBAB_2$. We note that the $SABA_2$ and $SBAB_2$ integrators involve only forward steps which increases their numerical stability, while, the addition of the corrector results to better accuracy of the schemes, introducing simultaneously a small backward step.

1. Integration of the KG lattice

Hamiltonian (6) is suitable for the implementation of the $SABA_2C$ integration scheme since it attains form (A1) with

$$A \equiv \sum_{l=1}^{N} \frac{p_l^2}{2},$$

$$B \equiv \sum_{l=0}^{N} \frac{\tilde{\epsilon}_l}{2}u_l^2 + \frac{1}{4}u_l^4 + \frac{1}{2W}(u_{l+1}-u_l)^2,$$

$$\epsilon = 1, \quad \text{(A9)}$$

where N is the number of anharmonic oscillators. The operators $e^{\tau L_A}$, $e^{\tau L_B}$, and $e^{\tau L_C}$, which propagate the set of initial conditions (u_l,p_l) at time t, to their final values (u_l',p_l') at time $t+\tau$, with $l=1,2,\ldots,N$, are

$$e^{\tau L_A}:\begin{cases} u_l' = p_l\tau + u_l \\ p_l' = p_l, \end{cases} \quad \text{(A10)}$$

$$e^{\tau L_B}:\begin{cases} u_l' = u_l \\ p_l' = \left[-u_l(\tilde{\epsilon}_l+u_l^2)+\frac{1}{W}(u_{l-1}+u_{l+1}-2u_l)\right]\tau + p_l, \end{cases} \quad \text{(A11)}$$

$$e^{\tau L_C}:\begin{cases} u_l' = u_l \\ p_1' = 2\left\{\left(\frac{2}{W}+\tilde{\epsilon}_1+3u_1^2\right)\left[-u_1(\tilde{\epsilon}_1+u_1^2)+\frac{1}{W}(u_2-2u_1)\right]+\frac{1}{W}\left[u_2(\tilde{\epsilon}_2+u_2^2)-\frac{1}{W}(u_3+u_1-2u_2)\right]\right\}\tau + p_1 \\ p_l' = 2\left\{\frac{1}{W}\left[u_{l-1}(\tilde{\epsilon}_{l-1}+u_{l-1}^2)-\frac{1}{W}(u_{l-2}+u_l-2u_{l-1})\right]+\left[\frac{2}{W}+\tilde{\epsilon}_l+3u_l^2\right]\left[-u_l(\tilde{\epsilon}_l+u_l^2)+\frac{1}{W}(u_{l-1}+u_{l+1}-2u_l)\right]\right. \\ \qquad \left.+\frac{1}{W}\left[u_{l+1}(\tilde{\epsilon}_{l+1}+u_{l+1}^2)-\frac{1}{W}(u_{l+2}+u_l-2u_{l+1})\right]\right\}\tau + p_l, \quad \text{for } l=2,3,\ldots,N-1 \\ p_N' = 2\left\{\frac{1}{W}\left[u_{N-1}(\tilde{\epsilon}_{N-1}+u_{N-1}^2)-\frac{1}{W}(u_{N-2}+u_N-2u_{N-1})\right]+\left(\frac{2}{W}+\tilde{\epsilon}_N+3u_N^2\right)\left[-u_N(\tilde{\epsilon}_N+u_N^2)+\frac{1}{W}(u_{N-1}-2u_N)\right]\right\}\tau + p_N \end{cases} \quad \text{(A12)}$$

since

$$C = \sum_{l=1}^{N}\left[u_l(\tilde{\epsilon}_1+u_l^2)-\frac{1}{W}(u_{l-1}+u_{l+1}-2u_l)\right]^2 \quad \text{(A13)}$$

and $u_0=u_{N+1}\equiv 0$.

2. Integration of the DNLS lattice

We use the $SBAB_2$ integrator scheme to integrate the equations of motion (2), by splitting the DNLS Hamiltonian (1) as

$$A \equiv -\sum_{l=1}^{N}(\psi_{l+1}\psi_l^* + \psi_{l+1}^*\psi_l),$$

$$B \equiv \sum_{l=1}^{N}\epsilon_l|\psi_l|^2 + \frac{\beta}{2}|\psi_l|^4,$$

$$\epsilon = 1, \quad \text{(A14)}$$

with N being the number of lattice sites. The action of the operator $e^{\tau L_A}$ on ψ_l, with $l=1,2,\ldots,N$ at time t, leads to the computation of ψ_l' at time $t+\tau$ and includes three steps: (a) the transformation of the wave function from the real (ψ_l) to the Fourier (φ_q) space, through a fast Fourier transform

(FFT), (b) a rotation of φ_q, and (c) the inverse FFT of the wave function φ_q' evaluated at the previous step, i.e.,

$$e^{\tau L_A}:\begin{cases}\varphi_q = \sum_{m=1}^{N} \psi_m e^{2\pi i q(m-1)/N} \\ \varphi_q' = \varphi_q e^{2i\cos(2\pi(q-1)/N)\tau} \\ \psi_l' = \frac{1}{N}\sum_{q=1}^{N} \varphi_q' e^{-2\pi i l(q-1)/N}.\end{cases} \tag{A15}$$

On the other hand, the action of $e^{\tau L_B}$ on ψ_l reduces to a simple rotation in real space, namely,

$$e^{\tau L_B}:\{\psi_l' = \psi_l e^{-i(\epsilon_l+\beta|\psi_l|^2)\tau}\ . \tag{A16}$$

Note that for the DNLS model we do not apply the two corrector steps since the term $C=\{\{A,B\},B\}$ does not lead to an easily solvable system.

[1] P. W. Anderson, Phys. Rev. **109**, 1492 (1958).
[2] S. A. Gredeskul and Yu. S. Kivshar, Phys. Rep. **216**, 1 (1992).
[3] T. Schwartz, G. Bartal, S. Fishman, and M. Segev, Nature (London) **446**, 52 (2007).
[4] Y. Lahini, A. Avidan, F. Pozzi, M. Sorel, R. Morandotti, D. N. Christodoulides, and Y. Silberberg, Phys. Rev. Lett. **100**, 013906 (2008).
[5] D. Clement, A. F. Varon, J. A. Retter, L. Sanchez-Palencia, A. Aspect, and P. Bouyer, New J. Phys. **8**, 165 (2006); L. Sanchez-Palencia, D. Clement, P. Lugan, P. Bouyer, G. V. Shlyapnikov, and A. Aspect, Phys. Rev. Lett. **98**, 210401 (2007); J. Billy, V. Josse, Z. Zuo, A. Bernard, B. Hambrecht, P. Lugan, D. Clement, L. Sanchez-Palencia, P. Bouyer, and A. Aspect, Nature (London) **453**, 891 (2008); G. Roati, C. D'Errico, L. Fallani, M. Fattori, C. Fort, M. Zaccanti, G. Modugno, M. Modugno, and M. Inguscio, *ibid.* **453**, 895 (2008).
[6] D. L. Shepelyansky, Phys. Rev. Lett. **70**, 1787 (1993).
[7] M. I. Molina, Phys. Rev. B **58**, 12547 (1998).
[8] A. S. Pikovsky and D. L. Shepelyansky, Phys. Rev. Lett. **100**, 094101 (2008).
[9] I. García-Mata and D. L. Shepelyansky, Phys. Rev. E **79**, 026205 (2009).
[10] G. Kopidakis, S. Komineas, S. Flach, and S. Aubry, Phys. Rev. Lett. **100**, 084103 (2008).
[11] S. Flach, D. O. Krimer, and C. Skokos, Phys. Rev. Lett. **102**, 024101 (2009).
[12] O. Morsch and M. Oberthaler, Rep. Prog. Phys. **78**, 179 (2006).
[13] Yu. S. Kivshar and G. P. Agrawal, *Optical Solitons: From Fibers to Photonic Crystals* (Academic Press, Amsterdam, 2003).
[14] B. Kramer and A. MacKinnon, Rep. Prog. Phys. **56**, 1469 (1993).
[15] A. D. Mirlin, Phys. Rep. **326**, 259 (2000).
[16] A. A. Ovchinnikov, N. S. Erikhman, and K. A. Pronin, *Vibrational-Rotational Excitations in Nonlinear Molecular Systems* (Kluwer Academic/Plenum Publishers, New York, 2001).
[17] Yu. S. Kivshar and M. Peyrard, Phys. Rev. A **46**, 3198 (1992); Yu. S. Kivshar, Phys. Lett. A **173**, 172 (1993); M. Johansson, Physica D **216**, 62 (2006).
[18] J. Laskar and P. Robutel, Celest. Mech. Dyn. Astron. **80**, 39 (2001).
[19] S. Flach and C. R. Willis, Phys. Rep. **295**, 181 (1998); S. Flach and A. V. Gorbach, *ibid.* **467**, 1 (2008).
[20] C. Albanese and J. Fröhlich, Commun. Math. Phys. **138**, 193 (1991); G. Kopidakis and S. Aubry, Phys. Rev. Lett. **84**, 3236 (2000); Physica D **130**, 155 (1999); **139**, 247 (2000); J. Bourgain and W.-M. Wang, J. Eur. Math. Soc. **10**, 1 (2008); N. K. Efremidis and K. Hizanidis, Phys. Rev. Lett. **101**, 143903 (2008).
[21] D. M. Basko, I. L. Aleiner, and B. L. Altshuler, Ann. Phys. (N.Y.) **321**, 1126 (2006).
[22] L. Nadolski, Ph.D. thesis, Paris XI Université, 2001 (unpublished); L. Nadolski and J. Laskar, *Proceedings of the European Particle Accelerator Conference EPAC02*, 2002, p. 1276; Ch. Skokos and Y. Papaphilippou, *Proceedings of the European Particle Accelerator Conference EPAC08*, 2008, p. 682.